nELISA: A high-throughput, high-plex platform enables quantitative profiling of the secretome

Milad Dagher[1,4,5,*], Grant Ongo[1], Nathaniel Robichaud[1], Jinglin Kong[1,4,5], Woojong Rho[1,4,5], Ivan Teahulos[1,4,5], Arya Tavakoli[1], Samantha Bovaird[1], Shahem Merjaneh[1], Andrew Tan[1], Kiran Edwardson[1], Christelle Scheepers[1], Andy Ng[4,5], Andy Hajjar[1], Baly Sow[1], Michael Vrouvides[1], Andy Lee[1], Philippe DeCorwin-Martin[1], Shafqat Rasool[1], JiaMin Huang[1], Timothy Erps[1], Spencer Coffin[1], Yu Han[2], Srinivas Niranj Chandrasekaran[2], Lisa Miller[3], Maria Kost-Alimova[3], Adam Skepner[3], Shantanu Singh[2], Anne E. Carpenter[2], Jeffrey Munzar[1,4,5], David Juncker[4,5,*]

[1] Nomic Bio, Montreal, QC, Canada
[2] Broad Institute of MIT and Harvard, Imaging Platform, Cambridge, MA, USA
[3] Broad Institute of MIT and Harvard, Center for the Development of Therapeutics, Cambridge, MA, USA
[4] McGill Genome Centre, Montreal, QC, Canada
[5] Biomedical Engineering Department, McGill University, Montreal, QC, Canada
* Correspondence: milad@nomic.bio; david.juncker@mcgill.ca

Abstract

We present the nELISA, a high-throughput, high-fidelity, and high-plex protein profiling platform. DNA oligonucleotides are used to pre-assemble antibody pairs on spectrally encoded microparticles and perform displacement-mediated detection. Spatial separation between non-cognate antibodies prevents the rise of reagent-driven cross-reactivity, while read-out is performed cost-efficiently and at high-throughput using flow cytometry. We assembled an inflammatory panel of 191 targets that were multiplexed without cross-reactivity or impact on performance vs 1-plex signals, with sensitivities as low as 0.1pg/mL and measurements spanning 7 orders of magnitude. We then performed a large-scale secretome perturbation screen of peripheral blood mononuclear cells (PBMCs), with cytokines as both perturbagens and read-outs, measuring 7,392 samples and generating ~1.5M protein datapoints in under a week, a significant advance in throughput compared to other highly multiplexed immunoassays. We uncovered 447 significant cytokine responses, including multiple putatively novel ones, that were conserved across donors and stimulation conditions. We also validated the nELISA's use in phenotypic screening, and propose its application to drug discovery.

Introduction

Proteins are the major effector class of biomolecules and executors of biological function. Therefore, accurate quantification of proteins is essential for understanding the state of a biological system, as well as for translating these insights into new diagnostic, prognostic and treatment strategies [1]. While both genomics and transcriptomics have been interpreted as a proxy for protein profiling, their use in this context has serious limitations due to post-transcriptional regulation, differential translation rates, protein degradation, and spatiotemporal regulation, among other phenomena [1]. This highlights the need for protein profiling methods that can provide a truer representation, and more direct observation, of biology. However, the advent of proteomic tools has lagged due to multiple unique challenges with proteins, such as the large dynamic ranges at which they are present, their overall instability, the existence of multiple proteoforms, and the lack of straightforward amplification avenues such as PCR. As a result, scientists continue to lack broadly-applicable protein profiling tools that can scale without compromising fidelity, precision, throughput, and, perhaps most importantly, cost.

Significant efforts have been dedicated to scaling proteomics [1]. Mass spectrometry (MS)-based proteomics can be useful for discovery in many contexts, providing quantitative information for thousands of proteins and their post-translationally modified forms. However, MS has so far failed to overcome severe trade-offs between throughput and sensitivity, limiting its ability to scale, and tends to be biassed towards high abundance proteins [1]. The sandwich immunoassay, commonly known as the ELISA (enzyme linked immunosorbent assay), can be performed in high-throughput and remains a ubiquitous tool and approach for protein quantification from bench to clinic. Sandwich ELISAs are of special interest, being quantitative and highly specific due to the use of a capture antibody (cAb) to bind the analyte and detection antibody (dAb) to bind the analyte and generate a measurable signal. However, multiplexing ELISA systems to capture significant portions of the proteome has been limited by reagent-driven cross-reactivity (rCR), which severely jeopardises assay fidelity, even at low- to mid-plex levels [2]. In fact, rCR is the major barrier to multiplexing immunoassays beyond ~25-plex, resulting in many assay kits limiting content to ~10-plex. rCR is caused by the mixing of non-cognate antibodies, which are combined in solution and incubated together for target detection

[2,3]. This mixing enables combinatorial interactions between all antibodies and proteins, and allows the formation of mismatched sandwich complexes, which can be formed as a result of a single non-specific binding event. These non-specific interactions increase exponentially as the number of antibody pairs in solution multiply, increasing the background noise and thereby eroding assay sensitivity. This problem has for long limited the multiplexing of immunoassays to <50-plex, even with intensive selection of antibodies to minimise rCR [1,2,4].

Efforts to minimise rCR has resulted in commercially available platforms such as Olink's PEA technology [5], which does not prevent rCR but selectively reports bi-specific interactions using proximity-based DNA amplification of oligonucleotide pairs, and Somalogic's SomaScan [6], an aptamer platform where non-specific binding is minimised through multiple capture-release steps. Although these platforms allow more than 1,000 proteins to be measured in every assay, and are increasingly used, they are costly ($100s per sample) and have limited throughput and limited flexibility to measure a custom set of proteins. We previously reported methods to spatially array and separate miniature sandwich immunoassays so as to prevent antibodies from mixing and thus alleviating potential cross-reactivity [3,7,8]. However, lengthy spotting protocols and technical challenges increased cost and limited the reproducibility and throughput, resulting in similar limitations to PEA and SomaScan. Thus, a platform that achieves specificity at scale without compromising other parameters such as throughput, cost-efficiency, and versatility has yet to be developed.

Here, we introduce the nELISA, a next-generation multiplexed bead-based assay platform that combines two technologies to achieve high-fidelity multiplexing at scale. The first technology is CLAMP (colocalized-by-linkage assays on microparticles), which we introduce here for the first time. CLAMP is a novel sandwich assay design that completely prevents rCR by pre-immobilizing antibody pairs on the surface of microparticles, and detects target proteins using a novel detection-by-displacement approach, both of which are enabled by the use of DNA oligos. We combine CLAMP with a large-scale encoding and decoding approach to bead-based flow cytometry assays that we previously described [9], creating the nELISA. As a first demonstration of the nELISA, we built a 191-plex secretome panel that targets low-abundance cytokines, chemokines, and growth factors. We characterised the sensitivity, specificity and reproducibility of the platform, and illustrate its potential for high-throughput screening (HTS) by profiling 191 proteins in 7,392 samples in <1 week. We illustrate the ease with which the nELISA can be integrated to existing HTS workflows by combining it with Cell Painting for phenotypic screening of a reference compound set. Finally, we demonstrate that the nELISA recapitulates hundreds of expected immune phenotypes in a single experiment, while also revealing unexpected insights with direct implications for drug discovery and development.

Results

CLAMP: a miniaturised sandwich assay on microparticles that avoids rCR

To overcome the rCR and throughput limitations of multiplexed immunoassays, we developed the CLAMP, which miniaturises the ELISA assay at the surface of a bead (Fig. 1). The CLAMP departs from the classical sandwich ELISA in three key ways: 1) pre-assembly of antibody pairs; 2) releasable detection antibodies; 3) conditional signal generation. First, detection antibodies are pre-assembled on their respective capture antibody-coated beads using flexible and releasable DNA oligo tethers (Fig. 1a). Spatial separation between non-cognate antibody pairs, each immobilised on different beads, precludes non-cognate interactions. When samples are mixed with the beads, target proteins can be recognized simultaneously by the antibodies, forming a ternary sandwich complex (Fig. 1b). Second, the releasable tethering of the detection antibodies allows for their displacement by toehold-mediated strand displacement [10]. Thus, CLAMP uses a novel signal transduction mechanism with a detection-by-displacement protocol based on toe-hold mediated strand displacement (Fig. 1c). Third, detection of the fluorescently labelled displacement oligo results in conditional signal generation. Indeed, only target-bound sandwich complexes are both labelled by the fluorescent displacement oligo and remain bound at the surface of the bead. In contrast, non-displacement isn't associated with a fluorescent signal, whereas target absence, or non-specific interactions, result in washing away of the fluorescent signal, thus ensuring low background signal (Fig. 1d).

Of note, during the displacement step, detection antibodies released from the bead and present in solution are found at concentrations orders of magnitude lower than commonly used in sandwich assays, suppressing the formation of off-target complexes. Indeed, while the local concentrations at bead surfaces can be in the micromolar range, the use of a low number of target-specific microparticles, and the limited number of antibodies present at the surface of each bead, result in a bulk concentration of detection antibody in solution too low (<aM) to yield detectable off-target binding.

Thus, as a result of its unique structure and detection method, CLAMP inherently avoids reagent driven cross-reactivity in multiplexing.

The nELISA combines CLAMP with emFRET to achieve high levels of multiplexing and throughput

To fully leverage the multiplexing capacity unleashed by the rCR-free nature of the CLAMP, we combined it with our previously-developed fluorescent barcoding technique [9], which achieves large-scale encoding and precise multi-colour labelling of beads. The technique leverages an ensemble multicolour FRET (emFRET) model to achieve facile encoding and decoding despite stochastic multicolour energy transfer. The use of four fluorescent dyes with partially overlapping spectra at various concentrations enables distinction of >3,000 barcodes (data not shown), and can be further expanded via optimization or inclusion of additional dyes. As a result, the nELISA has the potential to profile thousands of proteins in each sample. Furthermore, the fluorescence-based readout enables the use of high-throughput flow cytometry, and the use of 384-well plates to achieve high-throughput protein profiling. We developed workflows enabling 1,536 wells to be analysed daily on a single cytometer, the highest throughput of any highly-multiplexed immunoassay achieved to date, to the best of our knowledge.

Fidelity of assay performance is maintained at high-plex

To demonstrate high-fidelity multiplexing, we assembled a comprehensive secretome panel composed of 191 targets including cytokines, chemokines, and growth factors (Suppl. Table 1). Secreted proteins were chosen as the proof-of-concept set of proteins because they are simultaneously important to study, difficult to measure due to low abundance, and exhibit pleiotropic effects that depend on context and co-stimulations, therefore requiring broad profiling to better understand their roles [11]. To determine whether multiplexing had any negative effect on protein quantification, we ran a head-to-head measurement comparing signals generated in single-plex vs 191-plex. For individual proteins, calibration curves were indistinguishable; across the 191-plex panel, measurements correlated with an R^2 of 0.988 (Fig. 2b), showing that nELISA measurements are insensitive to multiplexing.

We then screened for rCR by running 'spike-one-in' testing, where each recombinant antigen was separately spiked to detect any cross-reactive detection by non-cognate CLAMPs (Fig. 2c). Of the 36,000+ possible cross-reactivities (where protein x is detected when protein y is spiked), we only detected 5; of these 3 were explained by shared epitopes. For example, it was expected that an IL-12 p40-specific CLAMP would detect IL-12 p70 and IL-23, as these heterodimers both contain the IL-12 p40 subunit. It was also expected that CXCL12α and CXCL12β CLAMPs would detect both CXCL12 isoforms, as they differ by only 4 residues. Unexpectedly, the CCL13 CLAMP detected CCL17, and the CCL3 CLAMP detected PCSK9. These cross-reactivities are presumed to be due to sample cross-reactivity (as opposed to rCR), whereby both antibodies detect the same off-target and would yield cross-reactive results even in a single-plex ELISA, and can be addressed by selecting alternative antibody pairs. Of note, detecting such cross-reactive events is a challenging and resource-intensive step for ELISA developers; our results suggest that the nELISA could be leveraged to accelerate and improve this process. We further validated nELISA specificity in more complex protein samples by running 'leave-some-out' testing, in which antigen pools lacking a subset of nELISA targets were profiled to ensure rCR remained low even in the presence of other abundant proteins in solution (Fig. 2d). These results establish the specificity and accurate quantification of our 191-plex secretome panel, demonstrating that the nELISA fidelity is unaffected by multiplexing, well beyond the traditional limit imposed by rCR.

Characterising dynamic range, sensitivity, and precision of nELISA

To further characterise the performance of the nELISA in 191-plex, we analysed standard curves generated for each nELISA target. nELISA yielded sigmoidal dose-response curves similar to classical ELISA and were robust, up to 100µg/mL tested here, against the Hook effect that can affect quantification at high target concentrations in some immunoassay formats [12] (Fig 2e). These characteristics enabled us to extend the dynamic range (xDR) of the assay by merging concentrations obtained from profiling proteins at 2 dilutions (see Methods), without impacting the assay throughput (Fig. 2e-f). Thus, high abundance proteins with concentrations up to 10 µg/mL could be quantified accurately. At the lower end of the detection spectrum, we analysed the sensitivity of the nELISA, and found limits of detection as low as 0.1 pg/mL (Fig. 2g) Assay binding range was generally governed by antibody affinities, as we observed concordance between CLAMP and classical ELISA formats. Combined with our xDR method, the nELISA

thus yielded a collective protein quantification range of 7 orders of magnitude, with each CLAMP possessing a dynamic range of 3-5 orders of magnitude (Suppl. Table 1).

Importantly, nELISA signals are highly reproducible. By measuring the same sample across wells, plates and profiling days, we calculated that the coefficient of variation (CV) of each CLAMP was ~3% well-to-well, and 5% plate-to-plate and day-to-day (Fig. 2h). As a result of variations much smaller than that of biological assays, the nELISA is inherently repeatable, enabling large scale cell-based screening. Furthermore, the nELISA includes several layers of controls that ensure signal stability over time (Suppl. Fig. 1). Thus, non-human targeting CLAMPs are added to every well as a Displacement Control, ensuring that CLAMPs do not yield signals in the absence of their target. In addition, Signal Normalisation Controls are added, consisting of CLAMPs lacking a detection antibody, and able to directly hybridise with the Detection Oligo. We also included controls on a separate calibration plate, consisting of standard curves of every CLAMP, as well as reference samples used for quality control. The performance of these controls is highly consistent over time, as shown by the tight overlap of standard curves performed on different days (Suppl. Fig. 2), as well as the reproducible quantification of targets in reference samples across 24 different nELISA runs, using 4 different lots of CLAMPs (Suppl. Fig. 3).

Benchmarking and validation against existing platforms

To validate the nELISA ability to quantify proteins from biological samples, we collected cell culture supernatants from peripheral blood mononuclear cells (PBMCs), which we profiled with the 191-plex nELISA, and with a 48-plex panel based on the commonly used multiplexed immunoassay platform, xMAP. Of the 36 targets shared by both platforms, 24 were detected in our samples by both platforms. Quantification of these targets revealed that xMAP and nELISA results correlated quite well, with a median Spearman correlation of 0.92 (Fig 2i, Suppl. Fig. 2). Leave-some-out testing revealed that targets correlating poorly between nELISA and xMAP displayed significant rCR in the xMAP platform as off-target protein concentrations approached 1ng/mL (Fig 2j). Taken together, these results demonstrate that the nELISA exhibits superior specificity, and is unique in its ability to achieve bona fide multiplexed quantification, where concentrations measured are not impacted by the level of multiplexing.

nELISA screening of peripheral blood mononuclear cell (PBMC) secretome characterises cytokine responses

To illustrate the utility of nELISA we chose to apply it to characterise cytokine responses and interactions in PBMCs. These cells provide a uniquely accessible cell population that can be controlled and stimulated in any number of experimental conditions. This flexibility of PBMCs can thus provide a wealth of information for diverse studies, such as functional genomics, where the tunable information provides significant advantages over snapshots available from profiling plasma/serum [13,14]. However, the diversity of conditions that can be tested also presents a major scaling challenge, as tracking PBMC cytokine responses at the protein level has so far been limited by high cost, limited throughput and limited content of available tools. While common, attempts to track cytokine responses by transcriptomics suffer from the limited correlation between mRNA and protein levels of cytokines due to extensive post-transcriptional and post-translational regulation.

To demonstrate the nELISA's ability to overcome these barriers, we selected 6 different PBMC donors to capture biological variability, which we treated with 4 different inflammatory stimuli at multiple doses. In addition, we used a small library of 80 recombinant human proteins with known immunomodulatory properties as "perturbagens" to further characterise immune responses (Fig 3a), generating 7,392 profiles of human cytokines, chemokines, and growth factors. Using UMAP as an overview of the entire nELISA dataset, distinct phenotypes clustered by stimulation condition, by PBMC donors, as well as by the concentration of stimulus used (Fig 3b). In addition, individual cytokine perturbagens with particularly strong effects created their own phenotypic clusters, including IL-4, IL-10, IL-1 RA/RN, IFNα2 and IFNβ (Fig 3b), demonstrating the power of the nELISA for phenotypic screening.

nELISA recapitulates classical immune responses

Using different stimulatory agents enables preferential stimulation of different subsets of cells (T cells vs myeloid cells) within PBMCs. Thus, primarily myeloid cell-derived proteins such as IL-1α and IL-1β increased in response to myeloid stimuli (Fig. 3c), whereas primarily T-cell derived proteins like IL-17A and IL-2 increased in response to T cell stimuli

(Fig. 3d); proteins expressed by multiple cell types such as TNFα and IFNγ increased in response to all stimuli (Fig 3c-d) [15]. Next, we analysed cytokine interactions, defined as changes in expression of a given PBMC-derived cytokine in response to a given recombinant cytokine perturbagen, in any or all of the stimulation conditions, across multiple donors (see Methods). Classical pro-inflammatory cytokines such as IFNγ and IL-1β were regulated by a variety of perturbagens, in a manner consistent with the expected role of each perturbagen (Fig 3e-f). For example, IFNγ increased in response to IFNα2/β, IL2, IL-18, Il-15, and IL-7, all powerful inducers of IFNγ [16–19], but was suppressed by IL-4, IL-10 [20,21].

To further establish that the nELISA can recapitulate expected biology, we compared the cytokine interaction responses found with the nELISA against CytoSig, a database of consensus, data-driven, cytokine-activity transcriptomic signatures [22]. Differences between mRNA and protein measurements notwithstanding, well-established immune responses were expected to be represented in both datasets and provide cross-validation. We found a total of 449 cytokine interactions using our nELISA data, and 137 cytokine interactions in PBMC data from CytoSig, of which 45 were detected by both platforms. Of these, 87% were in agreement with respect to directionality: 29 interactions resulted in increased cytokine production, and 10 resulted in repressed responses, in both nELISA and CytoSig (Fig. 3g). These included well known responses such as the induction by IFNγ of the IFNγ-inducible chemokines CXCL9 and CXCL10, and the potent immuno-stimulatory effects of IL-15, which induced both adaptive and innate immune mediators such as IFNγ, TNFα, CXCL9, CXCL10, CCL5, IL-17F, IL-22, and IL-1β, among others (Fig. 3g).

nELISA reveals cytokine interaction insights beyond transcriptomics

Interestingly, CytoSig data lacked many hallmark effects of Th1 and Th2 modulators. For example, the potent inhibitory effect of the Th2 cytokine IL-4 on IFNγ, TNFα and IL-1β was missing in the mRNA data, as was its ability to induce CCL22 and CCL24 [20,23–25]. In contrast, our nELISA data clearly showed these effects (Fig 3e). In fact, nELISA detected many more interactions in PBMCs than CytoSig (449 vs 137). Much of the difference stems from the inclusion of inflammatory stimuli in the nELISA dataset, enabling the detection of suppressive effects on cytokines with low baseline expression. As a result, CytoSig interactions are primarily increased expression (81%), whereas nELISA data is more balanced. This may explain why CytoSig fails to detect many of the potent anti-inflammatory effects of IL-10 on IFNγ, TNFα, IL-1β, IL-12 p40, CCL1, CCL3, CCL4, CCL5, CCL19, CXCL5, G-CSF, MMP-1, etc. [26] (Fig 3g).

Furthermore, CCL5, a particularly IFNγ-sensitive protein, was induced in the nELISA dataset by recombinant IFNγ and several conditions leading to increased IFNγ. However, its induction by IL-2, IL-7, IL-18, and IFNα2/β was not detected by CytoSig (Fig 3g). This may be due to post-transcriptional induction of CCL5 by IFNγ [27,28], or may reflect differences in experimental setup, such as temporal differences that would preclude detection of secondary effects by CytoSig. Similarly, post-transcriptional regulation likely explains differences in IL-1β regulation seen in nELISA vs CytoSig. Indeed, IL-1β is primarily regulated by cleavage and release of a pre-synthesized precursor, rather than de novo transcription [29], highlighting the necessity of protein-based detection to record changes. In line with this, IL-1β was the most responsive protein in the nELISA PBMC screen, responding to 35 distinct cytokine perturbagens, but only responding to IL-15 and IFNβ in the CytoSig database (Fig. 3g). This type of cytokine post-transcriptional regulation is likely the source of the disagreements between nELISA and CytoSig data. As seen in Figure 3g, there are 6 examples of a cytokine interaction resulting in a decrease in nELISA protein data, but an increase in CytoSig mRNA data. These interactions involve the expression levels of TNFα, IL-1α, CCL2, and CXCL1, all of which are well-studied examples of cytokines regulated at the level of translation into proteins, as well as mRNA stability, that could account for the observed differences [30–33]. Thus, while the nELISA recapitulates well established biology captured by gene expression databases such as CytoSig, our results suggest that it could provide a more accurate representation of cell signaling states at the population level than transcriptomics.

nELISA complements high-content phenotypic screening with mechanistic insights

Profiling the secretome using nELISA is compatible with a wide variety of cell-based assays, by first removing the cell supernatant for nELISA and using remaining cells for any cell-based assay of interest. In fact, combining nELISA with other multiplex profiling assays probing mRNA, chromatin, or morphology can greatly increase the information gained from a single sample. We tested the nELISA in combination with Cell Painting, a high-content imaging assay that quantifies phenotypes of cells stained with six dyes that label eight cellular components, and extracts thousands of

image-based features to form an image-based profile of the sample [34]. Using samples of A549 cells (human lung adenocarcinoma) prepared by the JUMP-Cell Painting Consortium [35], we measured secretome profiles from the exact same samples that were then Cell Painted. These cells were treated with a library of 306 well characterised compounds from the Broad Institute's drug repurposing library, with extensive annotations on their gene targets and mechanisms of action (MOA) [36].

To investigate the ability of each assay to identify compounds with shared MOA and gene targets, we first sought to leverage their existing annotations. We determined the "self-retrieval" of each compound on both platforms, representing the ability of replicate wells of a compound treatment to differentiate each other's phenotypes from that of control (DMSO-treateed) wells. Said differently, compounds with high self-retrieval yield a strong and distinct enough impact on the measured phenotype as compared to control wells. Among compounds resulting in significant self-retrieval, nELISA and Cell Painting were able to retrieve the known MOA and gene target information (according to available compound annotations) based on shared phenotypes. MOA-retrieval rates were 21-27% and gene target retrieval rates were 15-16% on both platforms. More total compounds were self-retrieved by Cell Painting, which was expected due to the limited secretory capacities of A549 cells and the absence of immune stimulation (Suppl. Fig. 5). Interestingly, while some compounds were well predicted by both platforms, each provided better predictions for distinct subsets of compounds, resulting in retrieval of an additional 33% of MOAs by adding nELISA to Cell Painting, highlighting their complementary nature (Suppl. Fig. 5). One caveat to this analysis is that the annotations are imperfect and do not fully capture a compound's biological effects. Indeed, nELISA identified at least one case where a compound displayed a distinct phenotype from other compounds in the MOA class "CDK inhibitors"; we discovered that its unique specificity for CDK4 [37] yielded opposite effects on the secretome as compared to the other compounds in that MOA class (Suppl. Fig. 6). Thus, we validated our ability to run two richly informative profiling assays on the same physical samples, and to cluster individual chemical perturbagens according to their mechanism of action or gene target.

To enable exploring compounds' relationships in an unbiased manner, without needing extensive annotations, we re-analyzed the nELISA dataset based on the similarity of the cytokine response profiles, without a priori knowledge of MOAs or gene targets (see Methods). This approach yielded additional mechanistic insights. For example, CHK inhibitors AZD7762 and 7-hydroxystaurosporine clustered closely, as did the Aurora B/C kinase inhibitor GSK1070916 (Suppl. Fig. 7). Consistent with the position of Aurora B downstream of CHK1 [38], the effect of GSK1070916 on A549 secretome partially recapitulated the effects of CHK inhibition, reducing the expression of IL-11, CXCL16, TNF RI, FLRG, and inducing MIF expression (Suppl. Fig. 7). Interestingly, pan-Aurora kinase inhibitors AMG900 and danusertib did not result in similar expression profiles, supporting the distinct mechanism of action of these inhibitors compared to GSK1070916 [39]. Overall, we found many examples where nELISA data complemented Cell Painting data for MOA elucidation.

nELISA profiles reveal cytokines with shared response profiles

To test whether the nELISA can reveal cytokines yielding similar responses independently of donor/stimulation conditions, we adapted our response profile similarity analysis pipeline to our PBMC screen. We calculated the fold change in expression of each protein in our 191-plex panel, in response to each of the cytokine perturbagens, across all donors within a stimulus condition (Suppl. Fig. 8). We also compiled effects across all stimulation conditions to capture the most reproducible perturbagen effects. UMAP clustering highlighted the most similar perturbagens (Fig 4a), with the protein expression patterns underlying these clusters shown in Fig 4b. It should be noted that some of our observations may derive from the purity of the recombinant proteins used, and the potential presence of bacterial contaminants; however, this effect is likely minor, as most cytokines cluster in predictable ways.

We observed that the classical Th1 and Th2 immune responses clustered around the prototypical cytokines IFNγ and IL-4, characterised by induction of IFNγ/CXCL10/CCL5, and CCL17/CCL22/CCL24, respectively (Fig 4a). The proximity of these clusters is explained by the shared inhibition of innate immune responses (ex: IL-1β, TNFα, G-CSF) as seen in Fig 4b. An additional cluster that shared the suppression of IL-1β/TNFα, but had little to no effect on the expression of other cytokines, was formed by recombinant C5/C5a, EMMPRIN, GDNF, MMP-3, MMP-7, uPA, PTX3, and the soluble form of FAS-L. A distinct cluster was formed of cytokines whose main effect was to induce IFNγ expression; this included the interleukins IL-2, 7, 15, 18, 23, 27 as well as CXCL12β. Interestingly, CXCL12α clustered with another group of proteins whose main effect was to induce the secretion of IL-1β (Fig 4b). This is the largest group and included

IL-1α, LIF, IL-33, PDGF-BB, sCD40L, CCL21, TRAIL and IL-17C/D/F. The remaining clusters were formed by perturbagens either inducing TNFα, IL-10 and IL-1α/β, or blocking TNFα and/or CCL24.

nELISA uncovers cytokines with potential therapeutic implications

Interestingly, our analysis pipeline enabled us to highlight lesser known cytokine biology, such as chemotaxis-independent effects of chemokines [40]. Thus, CX3CL1, CCL1, CCL5, CCL11, CCL26, CXCL10, CCL24, CXCL12α/β and C5a all modulated the expression of cytokines such as IFNγ, TNFα, IL-1β, GM-CSF and IL-10, in the absence of a chemotactic gradient (Fig 4b, d). Furthermore, many of the expression changes regulated by chemokines are stimulation-dependent (Suppl. Fig. 8). These observations support a growing body of evidence for activities of chemokines beyond migration, involving signalling via distinct G-protein signals [41]. For example, CXCL12 has been described as a co-stimulatory signal for T cells functioning through G_q and G_{11}, rather than the G_i classically associated with chemotaxis [42]. Thus, the nELISA could provide critical information in the development of therapeutic chemokines.

Of note, nELISA clustering identified similarities between therapeutic cytokines, suggesting possible drug repurposing approaches. IL-1 Receptor antagonist (IL-1 RA/RN) and IFNβ clustered similarly based on their inhibition of innate immune responses, yet IL-1 RA/RN induced none of the pro-inflammatory cytokines induced by IFNβ, such as IFNγ and CXCL10 (Fig 4a-c). This may have implications in the treatment of multiple sclerosis (MS): indeed, IFNβ is a common treatment for MS that appears to function at least in part through increasing IL-1 RA/RN expression, but has flu-like side effects [43–45]. In contrast, recombinant IL-1 RA/RN (anakinra) is very well tolerated and is currently being evaluated for MS in a phase 1 clinical trial [46,47]. In our data, IL-1 RA/RN was induced by IFNβ, but itself displayed only anti-inflammatory effects. In fact, correlating the effect of adding IFNβ or IL-1 RA/RN to PBMCs demonstrates that IL-1 RA/RN can inhibit all of the same cytokines/chemokines as IFNβ, with the exception of CCL22 and CCL24, while additionally inhibiting the expression of cytokines induced by IFNβ thought to be detrimental to MS, such as IFNγ and CCL7 (Fig 4c). Thus, our screen provides support for using anakinra in MS, and highlights the power of nELISA protein profiling for drug discovery.

Discussion

Although high-throughput genomic and transcriptomic methods have led to major advances in our understanding of biological processes and the molecular basis of disease, high-throughput approaches for protein profiling have lagged behind. Here, we described the development of nELISA, a protein profiling assay that leverages CLAMP to overcome the rCR limitations seen with other multiplex immunoassay systems, enabling scaling of content to 191-plex. Bead-based miniaturisation of the sandwich immunoassay enabled flow cytometry-based detection, with current off-the-shelf technologies able to process samples at a rate of 60 minutes per 384-well plate [48], resulting in a throughput of up to ~10,000 samples per week. We demonstrate that the nELISA can scale immunoassays while maintaining or improving on their sensitivity, specificity, and dynamic range. In addition, the CLAMP format dramatically reduces the amount of detection antibodies consumed, relative to other multiplexing formats. As reagents are the main driver of the high cost associated with protein profiling tools, nELISA assays benefit from significant advantages in cost efficiency.

Given that protein-level information is a more accurate representation of cell states and function than transcriptomics, developing improved high-throughput methods for protein profiling is of critical importance. Here, we show that nELISA can deliver insights that may not be accessible at the mRNA level. For example, the key inflammatory mediator IL-1β was the most regulated protein in our screen; because it is primarily regulated at the post-translational level, these responses were not reflected in the CytoSig database and would not be expected to be captured by transcriptomic assays. Secondary effects are also more difficult to discriminate in transcriptomic datasets, as they preclude repeat sampling to separate early events from those occurring later. In contrast, secretome profiling is compatible with repeat sampling from the same well, enabling the tracking of cellular phenotypes over time and the deconvolution of primary effects from those further downstream. Such an experiment could enable unambiguous determination of whether CCL5 is induced downstream of IFNγ, which would require an unwieldy multiplication of samples for methods requiring cell lysis or fixation, such as transcriptomics.

We applied the nELISA to HTS, where we demonstrate that it can report on the activity of small molecules and recombinant proteins. In fact, we foresee that the nELISA could be used to characterise all kinds of perturbagens and cell types, including small CRISPR gene modulation, therapeutic antibodies, bi-specific engagers, and CAR T cells.

We have shown that the nELISA captures expected cellular phenotypes and biological interactions that provide critical insights for drug discovery. For example, in our PBMC assay, the clear separation of responses by donor suggests powerful uses for the nELISA in functional genomics if scaled to larger cohorts, as done in the Human Functional Genomics Project [13].

Importantly, we showed that nELISA can be easily combined with other cell-based assays, such as Cell Painting, to provide additional biological insights. nELISA and Cell Painting provided complimentary phenotypic insights, with the nELISA also providing mechanistic insight. This highlights the potential for combining nELISA with a wide range of cell-based assays, including transcriptomics, functional assays such as cell killing assays common in immuno-oncology settings, or cell surface staining experiments prevalent in immunology, to cost-effectively generate additional information from critical screens.

nELISA-based quantification of changes in the expression of secreted proteins in response to chemokines, as reported here, may have particularly useful applications in the development of therapeutic chemokines: indeed, screening with a chemotaxis assay is significantly more challenging, with lower throughput and signal-to-noise, than screening on the basis of changes in protein expression [49,50]. Should these changes in protein expression constitute bona fide markers of target engagement, they could be leveraged for many standard drug discovery applications that suffer from the limitations of chemotaxis assays, such as large combinatorial screens, SAR studies, pharmacodynamic studies, etc. Additionally, nELISA clustering could be used to identify similarities between therapeutic interventions, such as seen in the IL-1 RA/RN and IFNβ example described above, which may inform drug repurposing efforts.

In conclusion, the nELISA's high quality, uncompromising data at low cost will facilitate its adoption for high-throughput applications such as drug discovery. The self-contained nature of each CLAMP sensor, and the extensive barcoding universe accessible to the nELISA allows simple removal, exchange and as well as the addition of new sensors against new targets, and will enable the platform to expand well-beyond the 191-plex shown here, resulting in additional proteome coverage and new potential applications such as the detection of post-translational modifications, so long as antibodies are available. The 191-plex secretome panel described here serves to demonstrate the performance of the nELISA, and paves the way for eventual profiling of the secretome, as well as intracellular proteins, protein-protein interactions, and signalling pathways in a high-throughput, cost-effective manner for cells, organs-on-a-chip, organoids, and tissues alike.

Conflict of Interest Statement

The Authors declare the following competing interests: N.R., G.O., W.R., I.T., A.T., J.K., J.M., S.B., S.M., A.T., K.E., C.S., A.H., A.L., P.D.M., S.R., J.H., T.E., B.S., M.V., S.C. and M.D. are employees and have ownership interest in Nomic Bio, which markets the nELISA platform, D.J. has ownership interest in Nomic Bio. S.S. and A.E.C. serve as scientific advisors for companies that use image-based profiling and Cell Painting (A.E.C: Recursion, S.S.: Waypoint Bio, Dewpoint Therapeutics) and receive honoraria for occasional talks at pharmaceutical and biotechnology companies. All other authors declare no competing interests.

Acknowledgements

We thank Daniel Graham and Sarah Headland for their invaluable insights into the biology captured by nELISA profiling of PBMCs. We also thank the High-Throughput Screening Core Facility of the Institute for Research in Immunology and Cancer of the Université de Montréal for culturing and high-throughput screening of PBMCs.

Funding

Funding for this study was provided by Nomic Bio, the Natural Sciences and Engineering Research Council of Canada (NSERC) Discovery and I2I grants, as well as from the Consortium Québécois sur la Découverte du Médicament (CQDM), Healthy Brains Healthy Lives (HBHL) and GSK. The authors also acknowledge funding from the Massachusetts Life Sciences Center Bits to Bytes Capital Call program (to AEC) and the National Institutes of Health (R35 GM122547 to AEC). The authors also gratefully acknowledge the use of the PerkinElmer Opera Phenix® High-Content/High-Throughput imaging system at the Broad Institute, funded by S10 Grant NIH OD-026839.

Methods

Recombinant sample generation

Recombinant protein stocks and protein pools (Nomic Bio) were prepared in Sample Buffer, consisting of RPMI + 10% FBS, containing 1-191 proteins at 100ng/mL per protein. For standard curves in singleplex and in multiplex, individual protein stocks and protein pools were serially diluted in Sample Buffer from 100ng/mL to 0.1pg/mL per protein. For "Spike-1-in" assays, individual protein solutions were prepared at 10 ng/mL. For "Leave-some-out" assays, protein pools containing 130-191 proteins at 100 pg/mL per protein were prepared in Sample Buffer. Each pool contained either all the targets in the 191-plex panel, or lacked a subset of targets in the 191-plex panel. For cross-reactivity comparisons with xMAP, protein pool A4 was serially diluted from 200ng/mL to 0.1pg/mL (per protein), and aliquots were stored at -80oC for profiling by nELISA and xMAP platforms. For reproducibility testing, a reference cell culture supernatant sample was distributed across the wells of four 384-well plates; for each plate, nELISA profiling was performed on a different day, and variation was calculated across wells on the same day, and across plates on different days.

Cell culture

Frozen PBMCs from healthy donors (StemCell) were thawed in 37oC water bath and transferred to 50mL Falcon tube with 40mL pre-warmed medium (RPMI + 10%FBS), centrifuged 10min@200g, then resuspended in 10mL pre-warmed medium. Viability was assessed by trypan blue exclusion (>95% viability for all donors) and 50,000 viable cells (25uL at 2M cells/mL) were transferred to each well of a 384 well plate, containing 50uL per well of pre-warmed media +/- stimulus +/- perturbagens, and incubated for 24h at 37oC. Perturbagens (Nomic Bio) were present at 50ng/mL. For stimulation conditions, LPS (InvivoGen) was present at 5ng/mL, 100ng/mL or 2000ng/mL; PolyIC (InvivoGen) was present at 400ng/mL, 2,000ng/mL, or 10,000ng/mL; ConA (InvivoGen) was present at 5ng/mL, 2,500ng/mL or 12,500ng/mL; for PMA/i (InvivoGen), PMA was present at 100ng/mL or 500ng/ml, while ionomycin was present at 1ng/mL or 5ng/mL.

Preparation, incubation and collection of cell supernatants from PBMCs was performed at the High-Throughput Screening Core Facility of the Institute for Research in Immunology and Cancer of the Université de Montréal. After 24h, supernatants were collected, aliquots were frozen and shipped on dry ice for nELISA profiling at Nomic's facilities or xMAP profiling at EVE Technologies facilities.

A549 cell culture was performed at the Broad Institute's Center for the Discovery of Therapeutics (CDoT). Cells were seeded in 4 replicate 384 well plates and cultured for 24h in DMEM + 10% FBS in the presence or absence of reference compound library. Compounds were present at a single dose (5uM). Supernatants were collected, frozen, and shipped on dry ice to Nomic's facilities for nELISA profiling. Cells were fixed and stained for Cell Painting as previously described [51].

Protein profiling

Samples of recombinant proteins or cell culture supernatants profiled using the nELISA were frozen and shipped on dry ice to Nomic's Montreal facilities and analysed using the Maxplex (191 targets) and standard protocols. Briefly, samples were thawed on ice and diluted as required with cell culture media, then mixed 1:1 with resuspended nELISA beads and incubated 3 hours at room temperature. Target-bound beads were washed with Wash Buffer, then resuspended in Assay Buffer. Displacement Oligo was added to beads and incubated 30 minutes at room temperature, followed by an additional wash and resuspension in Assay Buffer for readout by high-throughput cytometry (Bio-Rad ZE5 cell analyzer). Results were decoded using Nomic software. Samples profiled using the xMAP platform were shipped frozen to EVE technologies and analysed using the Human Multiplex Cytokine Array / Chemokine Array 48-Plex (HD48) and standard protocols. Standard curves for all targets were generated to derive pg/mL values from cytometry fluorescence units. To extend nELISA dynamic ranges, samples were profiled at 2 dilutions, 2X and 50X, and merged together before read-out by cytometry. Standard curves were extended by stitching the linear ranges of a real standard curve and a virtual, 25x diluted, standard curve. The sum of interpolated protein concentrations from the 2X and 50X dilutions was used to derive a single protein concentration for each sample.

Data analysis pipeline - Fold change analysis

To identify compounds with significant effects on A549 cells, we calculated the fold change in expression of each protein in the 191-plex over the levels in control wells. Proteins with a fold change > 1.5 and $p < 0.05$ by Student T-test in any sample were considered significant; considering the exploratory nature of the experiment, no statistical correction was performed for multiple testing. Using the median value of the significant responses, clustergrams with hierarchical

clustering were generated using cosine similarity (python package: seaborn). UMAPs of the median fold change values were generated using cosine similarity dimensions=2, spread=1.3, minimum distance=0.2, nearest neighbours=4,python package: scanpy).

To identify cytokine interactions in our PBMC assay, we accounted for stimulus- and donor-specific effects as follows. For each perturbagen in each stimulus/stimulus concentration condition, the median concentration of each secreted protein across donors was divided by the median concentration of donors in the same stimulus/stimulus concentration condition, but the absence of perturbagen, to obtain the fold change of all targets in response to all perturbagens in each condition. Significant cytokine interactions were defined by a fold change > 1.5 and $p < 0.05$ by Student T-test; considering the exploratory nature of the experiment, no statistical correction was performed for multiple testing. In addition, for all significant cytokine interactions, the median fold change across all stimulation conditions was calculated to identify cytokine interactions common across stimulus conditions. Clustergrams with hierarchical clustering were generated using cosine similarity and the default parameters included in the Seaborn python package. UMAPs were generated using cosine similarity with dimensions=2, spread=0.9, minimum distance=0.8, nearest neighbours=4 and the scanpy python package.

To correlate significant cytokine interactions with the CytoSig database, we identified recombinant perturbagens and responding genes/proteins that were shared in both datasets to limit comparisons to shared experimental conditions. We also limited comparisons to experiments compiled in CytoSig that were generated using PBMCs to avoid cell-type specific distinctions. Furthermore, only “high confidence” datasets were included in our analysis. For each cytokine interaction, consisting of a recombinant perturbagen and a resulting significant Fold Change in the expression of a PBMC-derived cytokine, nELISA and CytoSig results were correlated.

Evaluating retrieval performance of nELISA and Cell Painting

We use average precision (AP) to report the ability of nELISA and Cell Painting to predict chemical mechanisms of action. Average precision is an information retrieval metric that evaluates the effectiveness of a ranking system by calculating how accurately the system ranks items based on their relevance to a query.

We use average precision for two different tasks 1) the ability of each perturbagen to retrieve its own replicates from among negative control profiles (“self-retrieval”), and 2) the ability of each perturbagen to retrieve its sister compounds (i.e., compounds that share at least one common MOA or gene target) (“MOA retrieval” and “gene target retrieval”). We note that many compounds have multiple MOA and gene annotations rather than just one of each; in addition to the fact that annotations can be incorrect and incomplete, this makes the retrieval problem challenging and retrieval rates low for sets of compounds like ours that were not chosen for selectivity. Formally, AP is the weighted mean of precision values across all ks, where k is the number of neighbours for a given class. The definition of class varies – each *perturbation* is the class while computing AP for task 1, and each *MOA* or *gene targeted by the compound* is the class for computing AP for task 2.

We measure similarity between perturbations using cosine similarity and develop the rank-ordered similarity of all other samples to the query using this metric. Finally, we average AP per class, termed *mean Average Precision (mAP)* (for that class). For task 2, we first filter out those perturbations that cannot be retrieved relative to negative controls in task 1 and also remove classes with only a single member. To set the threshold, we first calculate the p-values of each mAP in task 1 using a permutation test; compounds with a significance level of less than 0.05 are discarded. We summarise the success rate of a task by calculating the fraction of classes that have a p-value > 0.05.

Contributions

M.D. and D.J. conceptualized the method. M.D., G.O., N.R., J.K., A.N, and J.M. developed the methodology and conceived the nELISA investigations. M.D., J.K., W.R., I.T., A.T., S.B., S.M., A.T., K.E., C.S, A.H., B.S., M.V., S.R., J.H., T.E, S.C., and J.M. performed the investigations. Y.H., S.N.C., L.M., M.K.-A., A.S, S.S., and A.E.C. conceived, developed, and performed the Cell Painting investigations and analyzed the associated data. G.O., A.L., and P.D.M. analyzed the nELISA data and developed associated software. M.D. and N.R. drafted the original manuscript. M.D., N.R., A.E.C, and D.J. reviewed and edited the manuscript. M.D. and D.J. acquired funding and supervised the study.

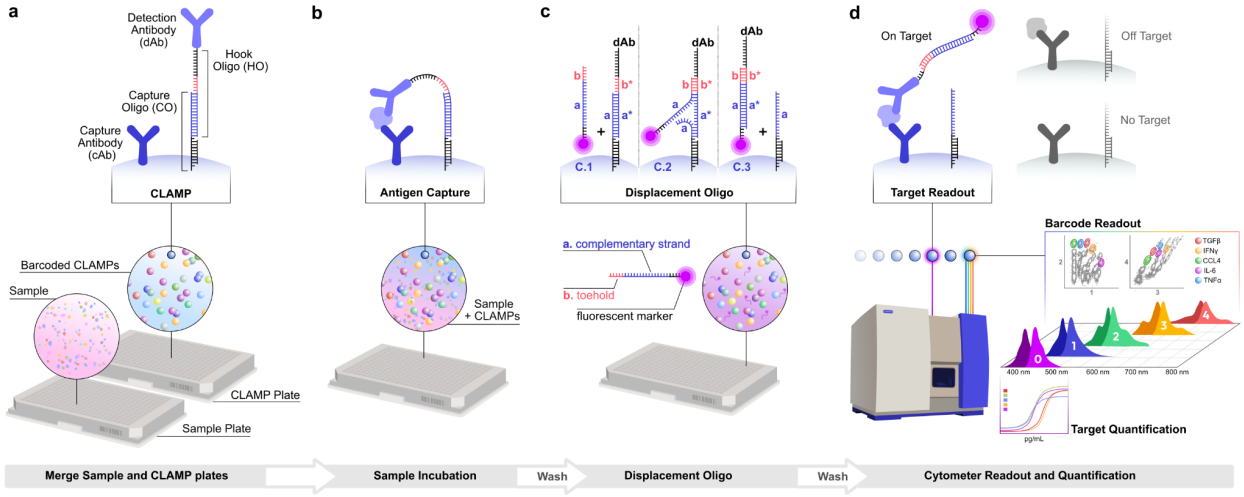

Figure 1. nELISA architecture and workflow. (a) A multiplexed nELISA is set up by pooling barcoded Colocalized assay-on-microparticles (CLAMPs) against different targets together. On each barcoded CLAMP, the detection antibody (dAb) is bound to a hook oligo (HO) that is tethered to the surface via partial hybridization with a capture oligo (CO) strand. (b) The assay is carried out by incubating the biological sample with barcoded CLAMPs generating sandwich binding in the presence of the target analyte only. (c) After washing, a fluorescently-labelled displacement oligo (DO) is added to displace HOs from their pre-hybridized COs via toe-hold mediated displacement, leading to (d) either labelling of the sandwich complexes that remain on the surface due to target presence and sandwich formation (left, in colour) or washing away of the dAb-DO hybrid in the absence of target or in the case of off-target binding (right, in grey). (bottom) Plate-based experimental workflow (from left to right): samples and nELISA beads in 384-well plates are combined, antigens are bound by cognate CLAMPs, displacement and labelling occurs on all beads in each well, followed by high-throughput flow cytometry of beads to reveal bead barcode and quantify target binding. Fluorescence spectra of detection dye (0) and barcoding dyes (1-4) are shown.

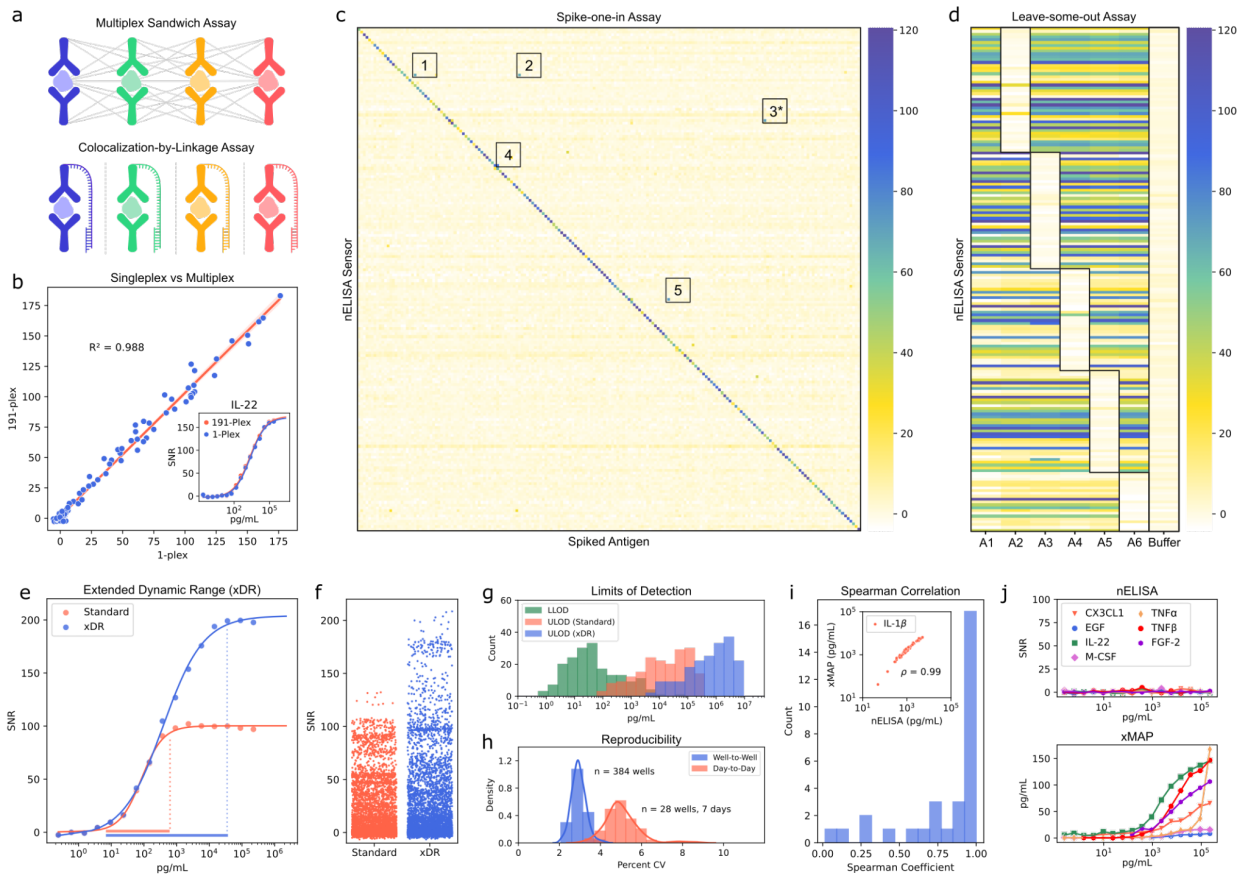

Figure 2: Characterization of nELISA specificity, sensitivity, and reproducibility. (a) Schematic representation of rCR in traditional multiplexed ELISAs, and its abrogation by CLAMP. (b) Correlation of SNR values for CLAMPs in 1-plex, or 191-plex format; an example standard curve is also shown (inset). (c) Spike-one-in assay: heatmap displays SNR values for each nELISA sensor in the 191-plex (y-axis) for each individually spiked antigen (x-axis); diagonal displays specific signals, cross-reactive events are numbered. (d) Leave-some-out assay: 6 pools of recombinant proteins consisting of either all the targets in the 191-plex panel (A1) or lacking a subset of targets (A2-A5) were profiled; outlined boxes indicate absence of target proteins; colours represent SNR. (e) Overlaid standard curves for 1 example CLAMP using (red) standard and (blue) extended dynamic range (xDR) protocols. (f) Distribution of SNR values for all 191-plex across 80 cell culture supernatants from stimulated PBMCs quantified using (red) standard or (blue) xDR protocols. (g) Distribution of the lower limits of detection (LLOD, green) and upper limits of detection (ULOD, red or blue) of 191 sensors using (red) standard or (blue) xDR protocols. (h) Distribution of coefficients of variation (%CV) of all nELISA sensors in repeat measurements of a single sample across wells in a single plate (well-to-well, blue) and across plates profiled on different days (day-to-day, red). (i) Cell culture supernatants from stimulated PBMCs were analysed with nELISA and xMAP platforms; shown are the distribution of spearman correlation coefficients for shared sensors with detectable protein concentrations, and an example of correlating IL-1β concentrations (inset). (j) Cross-reactivity comparison on xMAP and nELISA platforms: 100 recombinant antigens were pooled and spiked in cell culture media at increasing concentrations; shown are the quantification of 7 proteins not present in the sample using the nELISA (top) and xMAP (bottom).

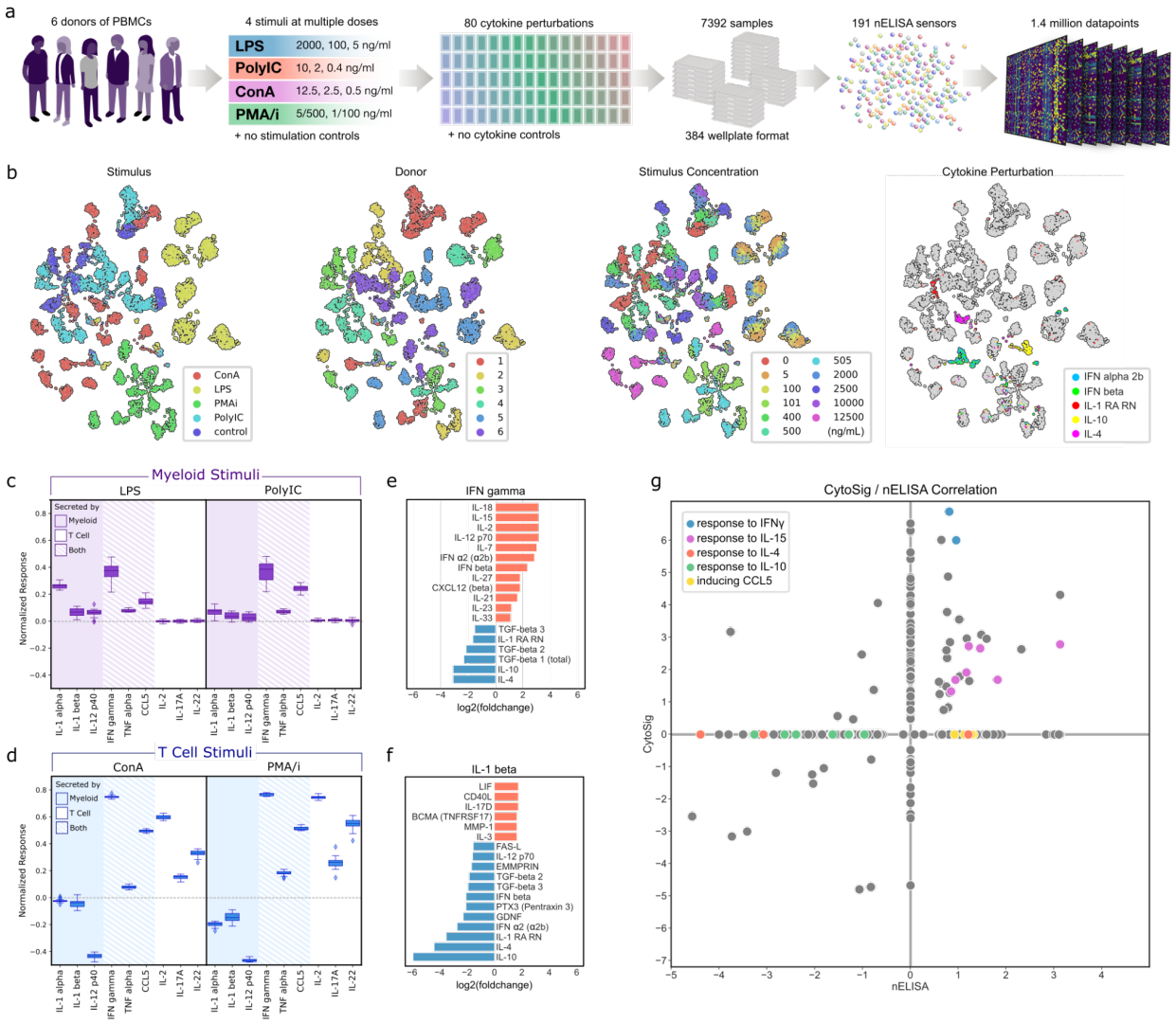

Figure 3: High-throughput nELISA screen captures PBMC phenotypic diversity and quantifies individual cytokine interactions. (a) Screen design: PBMCs isolated from 6 donors were treated with inflammatory stimuli at indicated concentrations, and further perturbed with 80 recombinant cytokine "perturbagens", generating a total of 7,392 samples; after 24 hours, concentrations of 191 secreted proteins were measured in the supernatant of each sample using the nELISA. (b) UMAP dimensionality reduction of the data; datapoints are coloured (from left to right) by stimulation condition, by donor, by stimulation concentration, or by individual cytokine perturbagens with strong effects, as indicated. (c) PBMC expression of indicated proteins, in response to myeloid stimuli (LPS or PolyIC), in the absence of recombinant cytokine perturbagens. Normalised signals represent differences in SNR compared to control wells. (d) PBMC expression of indicated proteins, in response to T cell stimuli (ConA or PMA/i), in the absence of recombinant cytokine perturbagens. (e-f) Fold change in the expression of IFNγ (e) and IL-1β (f) in response to indicated perturbagens, across all donors and stimulation conditions. (g) Correlation between cytokine interactions detected by nELISA and CytoSig in PBMCs, according to the fold change in expression of a protein in response to a perturbagen. Examples of cytokine interactions are indicated: response to IFNγ (blue), response to IL-15 (purple), response to IL-4 (red), response to IL-10 (green), perturbagens inducing CCL5 (yellow).

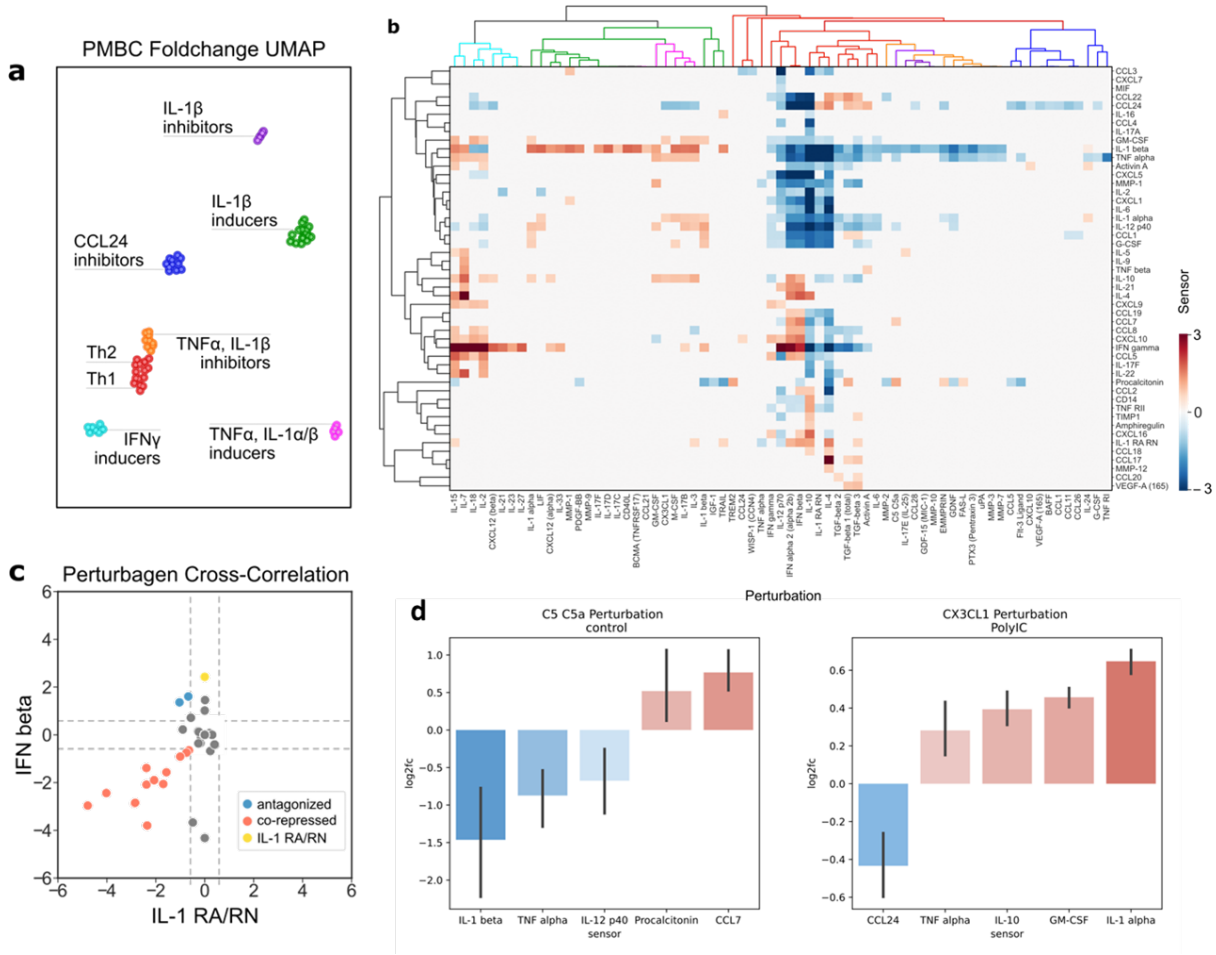

Figure 4: Clustering of cytokine profiles reveals phenotypically similar perturbagens and novel putative responses to recombinant chemokines. (a) UMAP of PBMC secretome phenotypes in response to perturbagens, compiled across all stimulation and donor conditions; clusters are labelled according to shared features in PBMC secretomes. (b) Heatmap dendrogram of perturbagen effects on cytokine expression across all stimulation and donor conditions; colours indicate fold change for each sensor over no perturbagen control. (c-d) Actionable insights emerging from nELISA profiling. (c) Applicability to drug repurposing, as seen by correlating significant effects of IFNβ and IL-1 RA/RN on unstimulated PBMCs. Shown are cytokines inhibited by both perturbagens (red), cytokines (IFNγ and CXCL10) induced by IFNβ but inhibited by IL-1 RA/RN (blue), and the induction of IL-1 RA/RN by IFNβ (yellow). (d) Markers of target engagement in response to chemokine perturbagens. Shown are the significantly regulated cytokines by C5a in otherwise unstimulated PBMCs (left), and by CX3CL1 in PBMCs stimulated with PolyIC (right).

References

1. Cayer, D. M., Nazor, K. L. & Schork, N. J. Mission critical: the need for proteomics in the era of next-generation sequencing and precision medicine. *Hum. Mol. Genet.* **25**, R182–R189 (2016).
2. Juncker, D., Bergeron, S., Laforte, V. & Li, H. Cross-reactivity in antibody microarrays and multiplexed sandwich assays: shedding light on the dark side of multiplexing. *Curr. Opin. Chem. Biol.* **18**, 29–37 (2014).
3. Pla-Roca, M. *et al.* Antibody colocalization microarray: a scalable technology for multiplex protein analysis in complex samples. *Mol. Cell. Proteomics* **11**, M111.011460 (2012).
4. Tighe, P. J., Ryder, R. R., Todd, I. & Fairclough, L. C. ELISA in the multiplex era: potentials and pitfalls. *Proteomics Clin. Appl.* **9**, 406–422 (2015).
5. Assarsson, E. *et al.* Homogenous 96-plex PEA immunoassay exhibiting high sensitivity, specificity, and excellent scalability. *PLoS One* **9**, e95192 (2014).
6. Gold, L., Walker, J. J., Wilcox, S. K. & Williams, S. Advances in human proteomics at high scale with the SOMAscan proteomics platform. *N. Biotechnol.* **29**, 543–549 (2012).
7. Laforte, V., Lo, P.-S., Li, H. & Juncker, D. Antibody Colocalization Microarray for Cross-Reactivity-Free Multiplexed Protein Analysis. *Methods Mol. Biol.* **1619**, 239–261 (2017).
8. Paquet-Mercier, F., Juncker, D. & Bergeron, S. Precise Chip-to-Chip Reagent Transfer for Cross-Reactivity-Free Multiplex Sandwich Immunoassays. *Methods Mol. Biol.* **2237**, 141–149 (2021).
9. Dagher, M., Kleinman, M., Ng, A. & Juncker, D. Ensemble multicolour FRET model enables barcoding at extreme FRET levels. *Nat. Nanotechnol.* **13**, 925–932 (2018).
10. Zhang, D. Y. & Winfree, E. Control of DNA strand displacement kinetics using toehold exchange. *J. Am. Chem. Soc.* **131**, 17303–17314 (2009).
11. Liu, G., Jiang, C., Lin, X. & Yang, Y. Point-of-care detection of cytokines in cytokine storm management and beyond: Significance and challenges. *View (Beijing)* **2**, 20210003 (2021).
12. Dodig, S. Interferences in quantitative immunochemical methods. *Biochem. Med.* 50–62 (2009).
13. Li, Y. *et al.* A Functional Genomics Approach to Understand Variation in Cytokine Production in Humans. *Cell* **167**, 1099–1110.e14 (2016).
14. Sen, P., Kemppainen, E. & Orešič, M. Perspectives on Systems Modeling of Human Peripheral Blood Mononuclear Cells. *Front Mol Biosci* **4**, 96 (2017).
15. Klegerman, M. E. & Plotnikoff, N. P. Lymphokines and Monokines. in *Biotechnology and Pharmacy* (eds. Pezzuto, J. M., Johnson, M. E. & Manasse, H. R.) 53–70 (Springer Netherlands, 1993).
16. Strengell, M. *et al.* IL-21 in synergy with IL-15 or IL-18 enhances IFN-gamma production in human NK and T

cells. *J. Immunol.* **170**, 5464–5469 (2003).

17. Borger, P., Kauffman, H. F., Postma, D. S. & Vellenga, E. IL-7 differentially modulates the expression of IFN-gamma and IL-4 in activated human T lymphocytes by transcriptional and post-transcriptional mechanisms. *J. Immunol.* **156**, 1333–1338 (1996).
18. Le, J., Lin, J. X., Henriksen-DeStefano, D. & Vilcek, J. Bacterial lipopolysaccharide-induced interferon-gamma production: roles of interleukin 1 and interleukin 2. *J. Immunol.* **136**, 4525–4530 (1986).
19. Kohno, K. *et al.* IFN-gamma-inducing factor (IGIF) is a costimulatory factor on the activation of Th1 but not Th2 cells and exerts its effect independently of IL-12. *J. Immunol.* **158**, 1541–1550 (1997).
20. Peleman, R., Wu, J., Fargeas, C. & Delespesse, G. Recombinant interleukin 4 suppresses the production of interferon gamma by human mononuclear cells. *J. Exp. Med.* **170**, 1751–1756 (1989).
21. D'Andrea, A. *et al.* Interleukin 10 (IL-10) inhibits human lymphocyte interferon gamma-production by suppressing natural killer cell stimulatory factor/IL-12 synthesis in accessory cells. *J. Exp. Med.* **178**, 1041–1048 (1993).
22. Jiang, P. *et al.* Systematic investigation of cytokine signaling activity at the tissue and single-cell levels. *Nat. Methods* **18**, 1181–1191 (2021).
23. Czimmerer, Z. *et al.* The epigenetic state of IL-4-polarized macrophages enables inflammatory cistromic expansion and extended synergistic response to TLR ligands. *Immunity* **55**, 2006–2026.e6 (2022).
24. Watanabe, K., Jose, P. J. & Rankin, S. M. Eotaxin-2 generation is differentially regulated by lipopolysaccharide and IL-4 in monocytes and macrophages. *J. Immunol.* **168**, 1911–1918 (2002).
25. te Velde, A. A., Huijbens, R. J., Heije, K., de Vries, J. E. & Figdor, C. G. Interleukin-4 (IL-4) inhibits secretion of IL-1 beta, tumor necrosis factor alpha, and IL-6 by human monocytes. *Blood* **76**, 1392–1397 (1990).
26. Saraiva, M., Vieira, P. & O'Garra, A. Biology and therapeutic potential of interleukin-10. *J. Exp. Med.* **217**, (2020).
27. Swanson, B. J., Murakami, M., Mitchell, T. C., Kappler, J. & Marrack, P. RANTES production by memory phenotype T cells is controlled by a posttranscriptional, TCR-dependent process. *Immunity* **17**, 605–615 (2002).
28. Homma, T. *et al.* Cooperative activation of CCL5 expression by TLR3 and tumor necrosis factor-alpha or interferon-gamma through nuclear factor-kappaB or STAT-1 in airway epithelial cells. *Int. Arch. Allergy Immunol.* **152 Suppl 1**, 9–17 (2010).
29. Dinarello, C. A. Overview of the IL-1 family in innate inflammation and acquired immunity. *Immunol. Rev.* **281**, 8–27 (2018).
30. Panganiban, R. P., Vonakis, B. M., Ishmael, F. T. & Stellato, C. Coordinated post-transcriptional regulation of the chemokine system: messages from CCL2. *J. Interferon Cytokine Res.* **34**, 255–266 (2014).
31. Korbecki, J., Barczak, K., Gutowska, I., Chlubek, D. & Baranowska-Bosiacka, I. CXCL1: Gene, Promoter,

Regulation of Expression, mRNA Stability, Regulation of Activity in the Intercellular Space. *Int. J. Mol. Sci.* **23**, (2022).

32. Fan, J., Heller, N. M., Gorospe, M., Atasoy, U. & Stellato, C. The role of post-transcriptional regulation in chemokine gene expression in inflammation and allergy. *Eur. Respir. J.* **26**, 933–947 (2005).
33. Freen-van Heeren, J. J. Post-transcriptional control of T-cell cytokine production: Implications for cancer therapy. *Immunology* **164**, 57–72 (2021).
34. Cimini, B. A. *et al.* Optimizing the Cell Painting assay for image-based profiling. *bioRxiv* 2022.07.13.499171 (2022) doi:10.1101/2022.07.13.499171.
35. Chandrasekaran, S. N. *et al.* JUMP Cell Painting dataset: morphological impact of 136,000 chemical and genetic perturbations. *bioRxiv* 2023.03.23.534023 (2023) doi:10.1101/2023.03.23.534023.
36. Corsello, S. M. *et al.* The Drug Repurposing Hub: a next-generation drug library and information resource. *Nat. Med.* **23**, 405–408 (2017).
37. Kubo, A. *et al.* The p16 status of tumor cell lines identifies small molecule inhibitors specific for cyclin-dependent kinase 4. *Clin. Cancer Res.* **5**, 4279–4286 (1999).
38. Zuazua-Villar, P., Rodriguez, R., Gagou, M. E., Eyers, P. A. & Meuth, M. DNA replication stress in CHK1-depleted tumour cells triggers premature (S-phase) mitosis through inappropriate activation of Aurora kinase B. *Cell Death Dis.* **5**, e1253 (2014).
39. Hardwicke, M. A. *et al.* GSK1070916, a potent Aurora B/C kinase inhibitor with broad antitumor activity in tissue culture cells and human tumor xenograft models. *Mol. Cancer Ther.* **8**, 1808–1817 (2009).
40. Rivas-Fuentes, S., Salgado-Aguayo, A., Arratia-Quijada, J. & Gorocica-Rosete, P. Regulation and biological functions of the CX3CL1-CX3CR1 axis and its relevance in solid cancer: A mini-review. *J. Cancer* **12**, 571–583 (2021).
41. Laufer, J. M. & Legler, D. F. Beyond migration-Chemokines in lymphocyte priming, differentiation, and modulating effector functions. *J. Leukoc. Biol.* **104**, 301–312 (2018).
42. Molon, B. *et al.* T cell costimulation by chemokine receptors. *Nat. Immunol.* **6**, 465–471 (2005).
43. Liu, J. S. H., Amaral, T. D., Brosnan, C. F. & Lee, S. C. IFNs Are Critical Regulators of IL-1 Receptor Antagonist and IL-1 Expression in Human Microglia. *The Journal of Immunology* vol. 161 1989–1996 Preprint at https://doi.org/10.4049/jimmunol.161.4.1989 (1998).
44. Comabella, M. *et al.* Induction of serum soluble tumor necrosis factor receptor II (sTNF-RII) and interleukin-1 receptor antagonist (IL-1ra) by interferon beta-1b in patients with progressive multiple sclerosis. *Journal of Neurology* vol. 255 1136–1141 Preprint at https://doi.org/10.1007/s00415-008-0855-1 (2008).

45. Sciacca, F. L., Canal, N. & Grimaldi, L. M. Induction of IL-1 receptor antagonist by interferon beta: implication for the treatment of multiple sclerosis. *J. Neurovirol.* **6 Suppl 2**, S33–7 (2000).

46. Ozdogan, H. *et al.* The efficacy of anti- IL-1 treatment in three patients with coexisting familial Mediterranean fever and multiple sclerosis. *Mult. Scler. Relat. Disord.* **45**, 102332 (2020).

47. Lopalco, G., Schiraldi, S., Venerito, V., Guerriero, S. & Iannone, F. Effectiveness and safety profile of anakinra in a HLA-B27 positive patient with multiple sclerosis-associated uveitis. *Mult. Scler. Relat. Disord.* **42**, 102152 (2020).

48. Wilson, R., Cossins, A. R. & Spiller, D. G. Encoded microcarriers for high-throughput multiplexed detection. *Angew. Chem. Int. Ed Engl.* **45**, 6104–6117 (2006).

49. Sai, J., Rogers, M., Hockemeyer, K., Wikswo, J. P. & Richmond, A. Chapter Two - Study of Chemotaxis and Cell–Cell Interactions in Cancer with Microfluidic Devices. in *Methods in Enzymology* (ed. Handel, T. M.) vol. 570 19–45 (Academic Press, 2016).

50. Das, A. & Yan, L. I. 6 - ANTI-CCL-2/MCP-1: DIRECTED BIOLOGICALS FOR INFLAMMATORY AND MALIGNANT DISEASES. in *Target Validation in Drug Discovery* (eds. Metcalf, B. W. & Dillon, S.) 103–119 (Academic Press, 2007).

51. Bray, M.-A. *et al.* Cell Painting, a high-content image-based assay for morphological profiling using multiplexed fluorescent dyes. *Nat. Protoc.* **11**, 1757–1774 (2016).